12 November 2010 | $10

Science

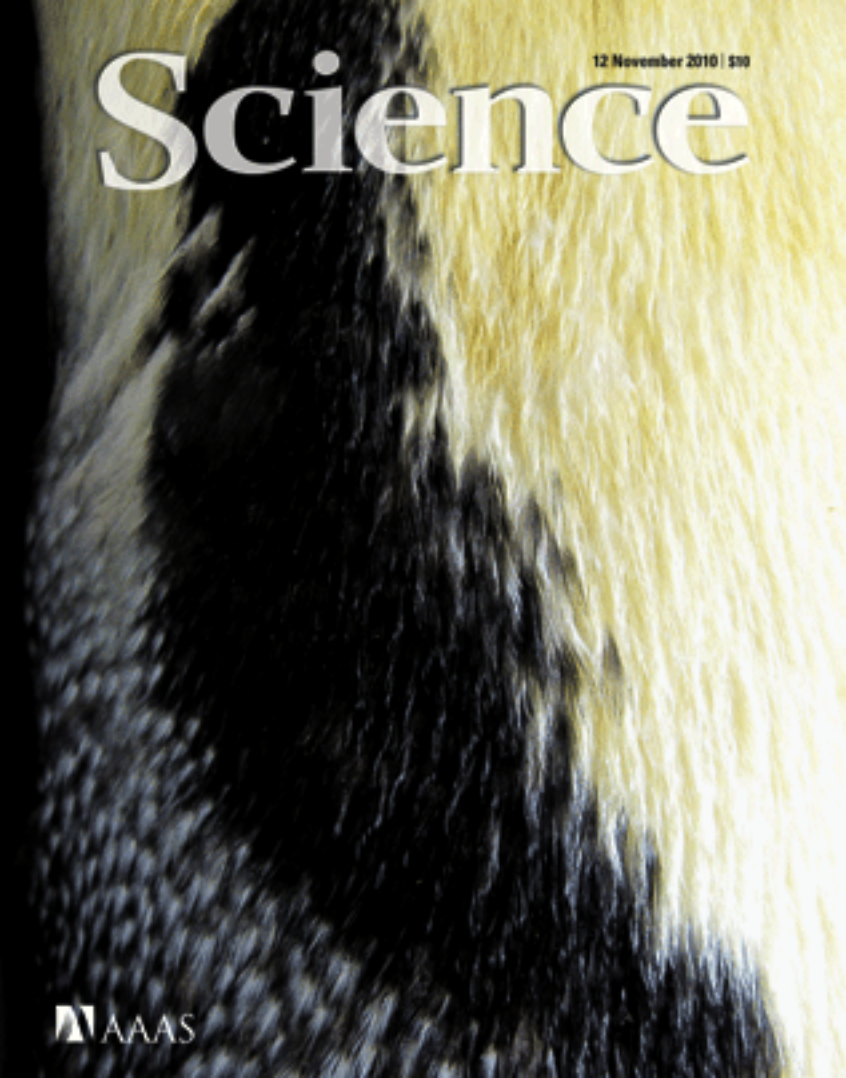

AAAS

Table 2. Chemical modes and amplitudes excited by pulses of N_2O, CO, and CH_4. The modes are identified with perturbation minus control (P − C) simulations. Amplitudes (*A*) are in globally integrated teragrams of N for N_2O and NOy and in teragrams for other species. The amplitudes of these modes are characterized by the amounts of N_2O (mode 1) and CH_4 (mode 2), shown in bold. Relatively small amplitudes are not shown (–).

P − C	Initial pulse	Mode (time)	*A* N_2O	*A* NOy	*A* CH_4	*A* O_3	*A* trop O_3
C2 − C1	10 Tg of N from N_2O	1 (108.4 years)	**+10.2**	+0.011	−2.1	−0.93	−0.01
		2 (12.5 years)	−0.002	–	**+2.8**	+0.11	0.03
C3 − C1	100 Tg of CO	1 (108.4 years)	**+0.0045**	–	–	–	–
		2 (12.5 years)	−0.005	−0.00003	**+7.4**	+0.30	+0.09
C4 − C1	10 Tg of CH_4	1 (108.4 years)	**+0.006**	–	–	–	–
		2 (12.5 years)	−0.007	-0.00004	**+9.85**	+0.40	+0.12

This N_2O-CH_4 coupling will shift with climate change over the 21st century. For example, the upper stratosphere cools as CO_2 increases, and this temperature change alters the N_2O-NOy-O_3 chemistry, reducing the impact of N_2O on O_3 (*21*). The importance of N_2O as an ozone-depleting substance (*22*) will thus be reduced, weakening the coupling described here but still maintaining the negative greenhouse feedback effect of CH_4 on N_2O emissions.

References and Notes

1. A. M. Fiore, J. J. West, L. W. Horowitz, V. Naik, M. D. Schwarzkopf, *J. Geophys. Res.* **113**, D08307 (2008).
2. M. Prather *et al.*, in *Climate Change 2001: The Scientific Basis. Third Assessment Report of the Intergovernmental Panel on Climate Change*, J. T. Houghton *et al.*, Eds. (Cambridge Univ. Press, Cambridge, 2001), pp. 239–287.
3. M. B. McElroy, J. C. McConnell, *J. Atmos. Sci.* **28**, 1095 (1971).
4. World Meteorological Organization (WMO), *Atmospheric Ozone 1985: Assessment of Our Understanding of the Processes Controlling Its Present Distribution and Change*, R. T. Watson *et al.*, Eds. (Global Ozone Research and Monitoring Project Report No. 16, WMO, Geneva, 1985).
5. J. Hsu, M. J. Prather, *Geophys. Res. Lett.* **37**, L07805 (2010).
6. Q. Tang, M. J. Prather, *Atmos. Chem. Phys.* **10**, 9681 (2010).
7. Materials and methods are available as supporting material on *Science* Online.
8. D. S. Stevenson *et al.*, *J. Geophys. Res.* **111**, D08301 (2006).
9. O. Wild, M. J. Prather, *J. Geophys. Res.* **105**, 24647 (2000).
10. R. G. Derwent, W. J. Collins, C. E. Johnson, D. S. Stevenson, *Clim. Change* **49**, 463 (2001).
11. M. J. Prather, *Geophys. Res. Lett.* **36**, L03811 (2009).
12. J. Hsu, M. J. Prather, O. Wild, *J. Geophys. Res.* **110**, D19305 (2005).
13. J. Hsu, M. J. Prather, *J. Geophys. Res.* **114**, D06102 (2009).
14. M. J. Prather, *Science* **279**, 1339 (1998).
15. D. L. Albritton, R. G. Derwent, I. S. A. Isaksen, M. Lal, D. J. Wuebbles, in *Climate Change 1994, Intergovernmental Panel on Climate Change*, J. T. Houghton *et al.*, Eds. (Cambridge Univ. Press, Cambridge, 1995), pp. 204–231.
16. M. J. Prather, *Geophys. Res. Lett.* **21**, 801 (1994).
17. M. Prather *et al.*, in *Climate Change 1994, Intergovernmental Panel on Climate Change*, J. T. Houghton *et al.*, Eds. (Cambridge Univ. Press, Cambridge, 1995), pp. 73–126.
18. P. Forster *et al.*, in *Climate Change 2007: The Physical Science Basis. Fourth Assessment Report of the Intergovernmental Panel on Climate Change*, S. Solomon *et al.*, Eds. (Cambridge Univ. Press, Cambridge, 2007), pp. 129–234.
19. WMO, *Scientific Assessment of Ozone Depletion: 2006*, C. A. Ennis, Ed. (WMO, Geneva, 2006).
20. K. L. Denman *et al.*, in *Climate Change 2007: The Physical Science Basis. Fourth Assessment Report of the Intergovernmental Panel on Climate Change*, S. Solomon *et al.*, Eds. (Cambridge Univ. Press, Cambridge, 2007), pp. 499–587.
21. J. E. Rosenfield, A. R. Douglass, *Geophys. Res. Lett.* **25**, 4381 (1998).
22. A. R. Ravishankara, J. S. Daniel, R. W. Portmann, *Science* **326**, 123 (2009).

23. This research was supported by NSF's Atmospheric Chemistry program (grant ATM-0550234) and NASA's Modeling, Analysis, and Prediction/Global Modeling Initiative program (grants NNG06GB84G and NNX09AJ47G).

Supporting Online Material

www.sciencemag.org/cgi/content/full/330/6006/952/DC1
Methods
References

9 August 2010; accepted 8 October 2010
10.1126/science.1196285

Fossil Evidence for Evolution of the Shape and Color of Penguin Feathers

Julia A. Clarke,[1]* Daniel T. Ksepka,[2,3] Rodolfo Salas-Gismondi,[4] Ali J. Altamirano,[4] Matthew D. Shawkey,[5] Liliana D'Alba,[5] Jakob Vinther,[6] Thomas J. DeVries,[7] Patrice Baby[8,9]

Penguin feathers are highly modified in form and function, but there have been no fossils to inform their evolution. A giant penguin with feathers was recovered from the late Eocene (~36 million years ago) of Peru. The fossil reveals that key feathering features, including undifferentiated primary wing feathers and broad body contour feather shafts, evolved early in the penguin lineage. Analyses of fossilized color-imparting melanosomes reveal that their dimensions were similar to those of non-penguin avian taxa and that the feathering may have been predominantly gray and reddish-brown. In contrast, the dark black-brown color of extant penguin feathers is generated by large, ellipsoidal melanosomes previously unknown for birds. The nanostructure of penguin feathers was thus modified after earlier macrostructural modifications of feather shape linked to aquatic flight.

During wing-propelled diving, penguins generate propulsive forces in a fluid environment ~800 times more dense and ~70 times more viscous than air (*1*). Recent fossil discoveries have yielded information on the sequence of early osteological changes in penguins accompanying the evolution of aquatic flight (*2*–*5*), but these specimens have not included feathers. Living penguin melanosome morphologies have not been described, although the melanin they contain is generally known to provide both color and wear-resistance to bird feathers (*6*–*8*). Here, we describe a giant fossil penguin with feathers recording preserved melanosome morphologies (*9*) and discuss the pattern and timing of major events in the evolution of penguin integument.

Systematic paleontology: Aves Linnaeus 1758 *sensu* Gauthier 1986. Sphenisciformes Sharpe 1891 *sensu* Clarke *et al.* 2003. *Inkayacu paracasensis* new gen. and sp. **Etymology:** *Inkayacu*—the Quechua, "Inka" for emperor and "yacu" for water; *paracasensis* for the Reserva Nacional de Paracas, Peru, the type locality. **Holotype**: MUSM 1444, a nearly complete skeleton with wing feathering, body contour feathers, and pedal scales (Figs. 1 to 3) (*10*). **Locality and horizon:** Upper Eocene of Yumaque Point, Paracas Reserve, Peru (*10*). **Diagnosis:** *Inkayacu paracasensis* is diagnosed by the following combination of characters (autapomorphies within Sphenisciformes demarcated by an asterisk): paired grooves meeting at midline on dorsal surface of premaxilla* (Fig. 1, GR), articular surfaces of otic and squamosal head of quadrate contacting one another,* furcula with blade-like hypocleidium,* conspicuous n. coracobrachialis sulcus developed on the humerus (Fig. 1, CNS), femur with widened and sharply distally tapering medial condyle* and tab-like process projecting from posterior intramuscular ridge at midshaft* (Fig. 1, MC and T), and weak proximal projection of cnemial crests of tibiotarsus (Fig. 1, CNE). See (*10*) for additional diagnosis, figures, and description.

[1]Department of Geological Sciences, University of Texas at Austin, Austin, TX 78712, USA. [2]Department of Marine, Earth, and Atmospheric Sciences, North Carolina State University, Raleigh, NC 27695–8208, USA. [3]Department of Paleontology, North Carolina Museum of Natural Sciences, Raleigh, NC 27601–1029, USA. [4]Departamento de Paleontología de Vertebrados, Museo de Historia Natural–Universidad Nacional Mayor de San Marcos (UNMSM), Lima 14, Perú. [5]Integrated Bioscience Program, University of Akron, Akron, OH 44325, USA. [6]Department of Geology and Geophysics, Yale University, New Haven, CT 06511, USA. [7]Burke Museum of Natural History and Culture, University of Washington, Seattle, WA 98195, USA. [8]Laboratoire des Mécanismes et Transferts en Géologie, Institut de Recherche pour de Développement, 14 Avenue Edouard Belin, F-31400 Toulouse, France. [9]Université de Toulouse, F-31400 Toulouse, France.

*To whom correspondence should be addressed: julia_clarke@jsg.utexas.edu

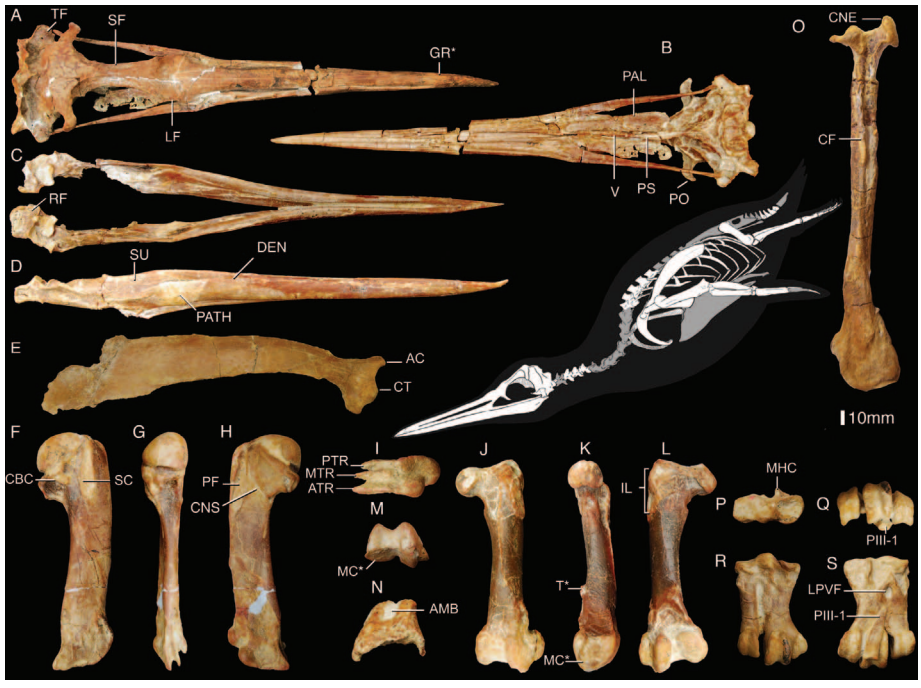

Fig. 1. Reconstruction of *Inkayacu paracasensis* in oblique anterior view showing recovered elements in white and photographs of the holotype specimen (MUSM 1444): skull and mandible in (**A** and **C**) dorsal, (**B**) ventral, and (**D**) lateral views; scapula in (**E**) lateral view and humerus in (**F**) posterior, (**G**) ventral, (**H**) anterior, and (**I**) distal views; femur in (**J**) dorsal, (**K**) medial, (**L**) ventral, and (**M**) distal views; patella in (**N**) anterior view; tibiotarsus in (**O**) lateral view; and tarsometatarsus in (**P**) proximal, (**Q**) distal, (**R**) anterior, and (**S**) plantar views. AC, acromion; AMB, pathway of m. ambiens tendon; ATR, anterior trochlear process; CBC, m. coracobrachialis caudalis insertion; CF, fibular crest; CNE, cnemial crests; CNS, coracobrachialis nerve sulcus; CT, coracoid tuberosity; DEN, dentary; GR, groove on premaxilla; IL, m. iliofemoralis and iliotrochantericus insertions; LF, lacrimal facet; LPVF, lateral proximal vascular foramen; MHC, medial hypotarsal crest; MC, medial condyle; MTR, middle trochlear process; PIII-1, manual phalanx III-1; PAL, palatine; PATH, pathology; PF, pectoralis fossa; PO, postorbital process; PS, parasphenoid rostrum; PTR, posterior trochlear process; SC, m. supracoracoideus insertion; SF, salt gland fossa; SU, surangular; T, tab-like process; TF, temporal fossa; V, vomer. Asterisks demarcate autapomorphies referenced in the diagnosis (*10*).

The holotype skeleton of *Inkayacu paracasensis* is disarticulated, with the exception of regions with extensive soft tissue impressions [distal left flipper (Fig. 2) and distal left pes (*10*)]. The fossil represents an animal with an estimated swimming length of 1.5 m. It has a hyper-elongate beak with a grooved tip and relatively gracile wing bones as compared with those of other giant penguins [such as *Icadyptes* (*11*)]. Conservative estimates of body mass for *Inkayacu* (~54.6 to 59.7 kg) are approximately twice the average mass of the Emperor Penguin (*12*); it is among the largest described fossil penguins (*10*).

Isolated contour feathers exhibit the broadened rachis of extant penguins. They grade from a light-colored (pale gray) base to a dark gray-black distal end (Fig. 3), where the rachis narrows and a cluster of distally directed, clumped darker barbs are developed at the tip. This coloration pattern is observed in penguins and other birds, resulting from increasing melanization toward the tip (*13*). Preserved portions of contour feathers and estimates from rachis diameter are consistent with a maximum length of approximately 3 cm, which is within the range of extant penguin body contour feathers (*10*) but notably shorter than contour feathers from several smaller-bodied extant high-latitude species (*10*). As in extant penguins, these feathers are pennaceous over most of their length; barbs are relatively evenly spaced, although barbule structure is not visible.

Preserved feathering along the left distal wing is exposed in dorsal view (Fig. 2) and appears to be close to life position with only slight peri-depositional posterior movement of the distal carpometacarpus. At the leading edge, texturing of a thin layer of gray matrix records the tips of tiny, closely packed covert feathers with melanosomes (Fig. 2, A to C). This darker layer continues over most of the carpometacarpus and distal radius. Where it split from the dorsal carpometacarpal surface, the underlying, light-colored matrix is textured with small regularly distributed raised knobs (Fig. 2A). Thin, paired impressions in this pale matrix preserve melanosomes (Fig. 2, D and E) that we interpret as melanized bases of the short,

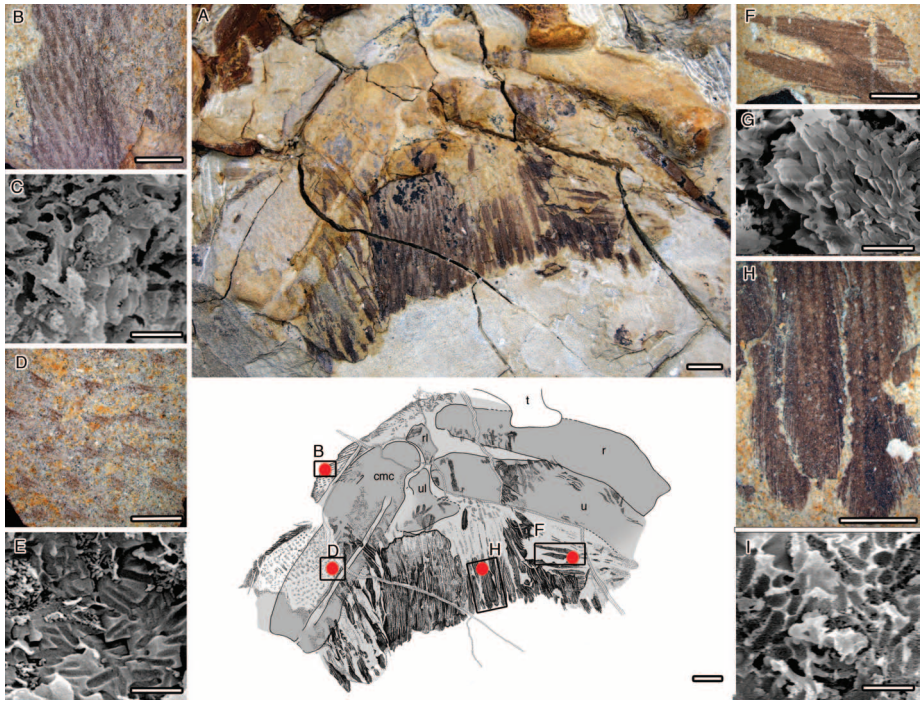

Fig. 2. The wing feathering of *Inkayacu paracasensis*. (**A**) Photograph and line drawing of the left wing (scale bar, 1 cm) showing location of insets and samples (circles) taken for scanning electron microscopy (SEM). (**B**) Close-up of the counterpart showing the surface of imbricated short covert feathers from the leading edge of the wing and (**C**) SEM of melanosomes in (B). (**D**) Close-up of the counterpart to the surface of the carpometacarpus with preserved melanized bases of covert feathers and (**E**) SEM of melanosomes from feather bases in (D) (melanosomes were not observed in surrounding matrix). (**F**) Close-up of tertiaries and (**G**) SEM of melanosomes in (F). (**H**) Secondaries and (**I**) SEM of melanosomes from (H). Scale bar for SEM images, 1 μm, and for insets, 3 mm. mc, carpometacarpus; r, radius; rl, radiale; t, tibiotarsus; u, ulna; ul, ulnare.

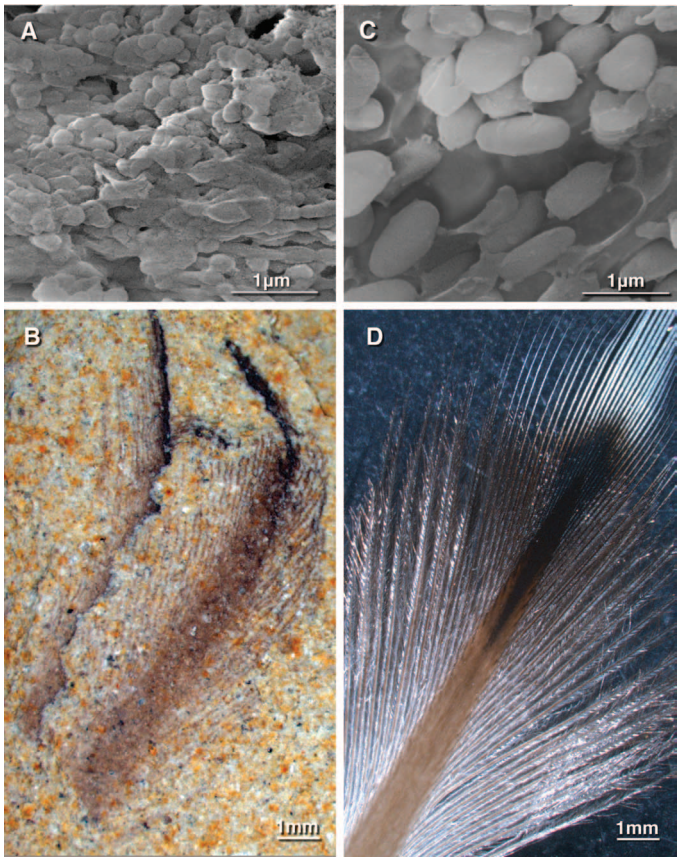

Fig. 3. Comparison of melanosome proportions and body contour feather morphology in (**A** and **B**) *Inkayacu paracasensis* and (**C** and **D**) representative extant penguins. (A) SEM of melanosomes preserved in the tip of (B) body contour feathers of *I. paracasensis*; (C) SEM of large, ellipsoidal melanosomes (shown, *Eudyptula minor*) from (D) similarly shaped body contour feathers (shown, *Aptenodytes forsteri*) in the penguin crown clade.

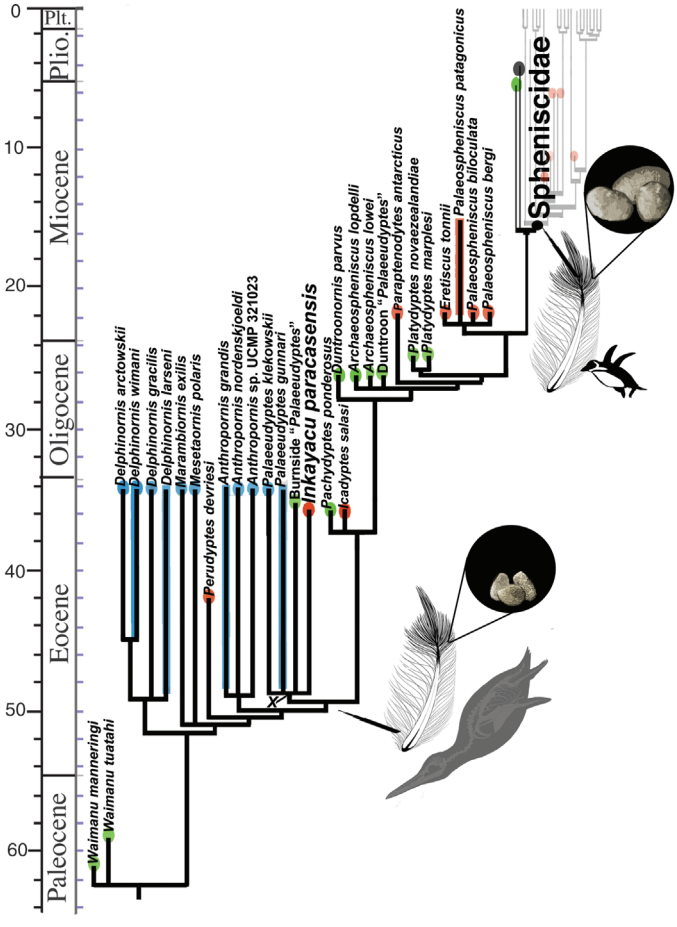

Fig. 4. Phylogenetic placement of *Inkayacu paracasensis* in a strict consensus cladogram of 45 most-parsimonious trees (MPTs) [Crown clade collapsed; see (*10*) for details of analysis]. Placement in a clade of Eocene giant penguins (X) implies an origin for the modified wing feathering, undifferentiated remiges, and broad rachis of body contour feathers (**insets**) no later than the early Eocene (*10*). Enlarged melanosomes are phylogenetically supported at minimum as a novelty of the penguin crown clade (**insets**). Stratigraphic distributions from (*5*). Fossil distributions are Antarctica, blue; New Zealand, green; Africa, dark gray; and South America, red.

darker-tipped covert feathers. Similarly, extant penguin coverts that exhibit dark tips are commonly white proximally but bear melanin stripes where the feathers enters the skin. The absence of melanosomes in the light matrix surrounding these marks in the fossil is consistent with similarly white proximal feathers (*9*) in *Inkayacu*. Presence of intact lesser covert feather bases and tips (in part and counterpart) represents a dimensionality rare in feather preservation.

Dorsal lesser-wing covert feathers partially overlie the distal wing bones (Fig. 2). Layers of elongate under-wing coverts pass ventral to the ulnare and carpometacarpus. The morphology and dark tonality of the feathers originating from the carpometacarpus and ulna, which comprise the trailing edge of the wing, are identical (Fig. 2, A and H). The homology of any one stacked layer of these feathers with the primaries and secondaries (remiges) of other birds is uncertain, but if one layer is considered to represent the remiges, at least one layer of coverts subequal in length must be present. All of these feathers show a broadened rachis and are relatively larger than in any extant penguin. The centers of rachises are light with darker edges. Many barbs are visible in distal feathers, and fewer are decipherable at midshaft. Seven incomplete feathers preserved in the matrix overlying the secondaries appear to be associated with the distal humerus.

All preserved feather types in *Inkayacu* record melanosomes (Figs. 2 and 3) (*10*) of dimensions within the range for avian taxa other than extant penguins (*10*). Although the length of extant penguin melanosomes was similar to other eumelanosomes, (mean of ~900 nm), their width (mean of ~440 nm) was far greater than all other Aves sampled (mean of ~300 nm) and in some cases approached their length (table S3). We thus analyzed them as a separate class in a discriminant analysis (*10*). We used four properties of melanosome morphology and distribution—long-axis variation, short-axis skew, aspect ratio, and density—to estimate the color predicted from the fossil feather samples (*10*). All six *Inkayacu* samples were assigned a gray or reddish-brown color with high probability, and none clustered with extant penguin samples.

The *Inkayacu* specimen provides evidence for an Eocene giant penguin clade (Fig. 4, Clade X) with a wide Southern Ocean distribution and for a third early-stem penguin dispersal to low latitudes (*11*). Phylogenetic analysis of a combined data set (*10*) finds the new species allied with three early- to late-Eocene species from New Zealand and Antarctica (*10*). The most recent common ancestor of *Inkayacu* and living penguins (Spheniscidae) is thus inferred to be present by the early Eocene and to have shared the lack of differentiation between stacked remiges and greater coverts, densely packed, squamiform lesser coverts, and broad flattened contour feather rachises seen in extant penguins. Early modifications in the wing feathering seen in *Inkayacu* created a narrow streamlined flipper and changed the hydrodynamic properties of the body feathers. Broad flat contour

feather rachises create less turbulent flow (*12*), which is an effect hypothesized to explain a lower observed drag coefficient than predicted from streamlined penguin body shape alone (*14*). They also facilitate reduction of intraplumage air (*15*). Most of the insulating properties of extant penguin contour feathers derive from their plumulaceous afterfeathers (*16*), which are not preserved or not present in *Inkayacu*.

Inkayacu shows that the large, subround melanosomes of extant penguin feathers were absent early in penguin evolution. At minimum, an increase in melanosome size and a decrease in their aspect ratio occurred after the early Eocene divergence of the clade that includes *Inkayacu* (Fig. 4, Clade X) and before the origin of extant penguins (Spheniscidae) by the late Miocene (*5*). The specific proportions of extant penguin melanosomes, the packing of these melanosomes into clusters within the barbs and rachis (*10*), and yellow, pterin-like pigmentation (*17*) are so far only known in the penguin crown clade.

Shifts in penguin plumage coloration indicated by the fossil may be linked to differences in ecology, thermoregulatory demands (*18*), or the more recent, predominantly Neogene, diversification of their primary mammalian predators (*19*, *20*). However, they do not explain the aberrant melanosome morphology associated with extant penguin brown-black color. Indeed, rather than selection for color, these changes may represent an unanticipated response to the hydrodynamic demands of underwater propulsion. Low aspect ratio, large size, and clustered melanosome distribution (*10*) may affect melanin packing and feather material properties. Melanin confers resistance to fracture (*6*, *21*, *22*), which is important to materials like feathers subjected to cyclical loading (*22*). Selective pressures for the color and material properties of penguin feathers could thus have led to nanoscale changes in melanosome morphology.

References and Notes

1. M. Denny, *Air and Water* (Princeton Univ. Press, Princeton, NJ, 1993).
2. R. E. Fordyce, C. M. Jones, in *Penguin Biology*, L. S. Davis, J. T. Darby, Eds. (Academic Press, San Diego, CA, 1990), pp. 419–226.
3. K. E. Slack *et al.*, *Mol. Biol. Evol.* **23**, 1144 (2006).
4. P. Jadwiszczak, *Polar Res.* **30**, 3 (2009).
5. D. T. Ksepka, J. A. Clarke, *Bull. Am. Mus. Nat. Hist.* **337**, 1 (2010).
6. E. H. Burtt Jr., *Ornithol. Monogr.* **38**, 1 (1986).
7. K. J. McGraw, in *Bird Coloration, vol.1, Mechanisms and Measurements*, G. E. Hill, K. J. McGraw (Harvard Univ. Press, Boston, 2006), pp. 243–294.
8. B. Stonehouse, *The Biology of Penguins* (Macmillan, London, 1975).
9. J. Vinther, D. E. G. Briggs, R. O. Prum, V. Saranathan, *Biol. Lett.* **4**, 522 (2008).
10. Materials and methods are available as supporting material on *Science* Online.
11. J. A. Clarke *et al.*, *Proc. Natl. Acad. Sci. U.S.A.* **104**, 11545 (2007).
12. B. Stonehouse, *Adv. Ecol. Res* **4**, 131 (1967).
13. W. L. N. Tickell, *Waterbirds* **26**, 1 (2003).
14. J. Lovvorn, G. A. Liggins, M. H. Borstad, S. M. Calisal, J. Mikkelsen, *J. Exp. Biol.* **204**, 1547 (2001).
15. R. P. Wilson, K. Hustler, P. G. Ryan, A. E. Burger, E. C. Noldeke, *Am. Nat.* **140**, 179 (1992).
16. C. Dawson, J. F. V. Vincent, G. Jeronimidis, G. Rice, P. Forshaw, *J. Theor. Biol.* **199**, 291 (1999).
17. K. J. McGraw *et al.*, *Pigment Cell Res.* **20**, 301 (2007).
18. H. M. Rowland, *Philos. Trans. R. Soc. London Ser. B Biol. Sci.* **364**, 519 (2009).
19. A. Berta, in *Encyclopedia of Marine Mammals, Second Edition*, W. Perrin, B. Würsing, J. G. M. Thewissen, Eds. (Academic Press, San Diego, CA, 2009), pp. 861–868.
20. U. Arnason *et al.*, *Mol. Phylogenet. Evol.* **41**, 345 (2006).
21. A. A. Voitkevich, *The Feathers and Plumage of Birds* (October House, New York, 1966).
22. R. H. Bonser, P. P. Purslow, *J. Exp. Biol.* **198**, 1029 (1995).

23. K. Browne helped produce the figures; W. Aguirre, P. Brinkman, and V. Schneider prepared the fossil. K. Middleton and M. Stucchi provided discussion. P. Unitt, K. Zyskowski, B. Wang, J. Tejada, J. Reyes, E. Díaz, and Z. Jiang provided professional assistance. The research was funded by the National Science Foundation (DEB-0949897 and DEB-0949899), the National Geographic Society Expeditions Council, the Air Force Office of Scientific Research (FA9550-09-1-0159), and University of Akron startup funds. MUSM 1444 is permanently deposited at the Museo de Historia Natural–UNMSM, Lima, Peru.

Supporting Online Material

www.sciencemag.org/cgi/content/full/science.1193604/DC1
Materials and Methods
SOM Text
Figs. S1 to S9
Tables S1 to S8
References
Phylogenetic Data Set

10 June 2010; accepted 10 September 2010
Published online 30 September 2010;
10.1126/science.1193604
Include this information when citing this paper.

Effects of Rapid Global Warming at the Paleocene-Eocene Boundary on Neotropical Vegetation

Carlos Jaramillo,[1]* Diana Ochoa,[1,2] Lineth Contreras,[3,1,4] Mark Pagani,[5] Humberto Carvajal-Ortiz,[6,1] Lisa M. Pratt,[6] Srinath Krishnan,[5] Agustin Cardona,[1] Millerlandy Romero,[1] Luis Quiroz,[1,7] Guillermo Rodriguez,[3,8] Milton J. Rueda,[9,3] Felipe de la Parra,[3] Sara Morón,[1,10] Walton Green,[1] German Bayona,[11,1] Camilo Montes,[1,11] Oscar Quintero,[12] Rafael Ramirez,[13] Germán Mora,[14] Stefan Schouten,[15] Hermann Bermudez,[16] Rosa Navarrete,[17] Francisco Parra,[18] Mauricio Alvarán,[16] Jose Osorno,[19] James L. Crowley,[20] Victor Valencia,[21] Jeff Vervoort[22]

Temperatures in tropical regions are estimated to have increased by 3° to 5°C, compared with Late Paleocene values, during the Paleocene-Eocene Thermal Maximum (PETM, 56.3 million years ago) event. We investigated the tropical forest response to this rapid warming by evaluating the palynological record of three stratigraphic sections in eastern Colombia and western Venezuela. We observed a rapid and distinct increase in plant diversity and origination rates, with a set of new taxa, mostly angiosperms, added to the existing stock of low-diversity Paleocene flora. There is no evidence for enhanced aridity in the northern Neotropics. The tropical rainforest was able to persist under elevated temperatures and high levels of atmospheric carbon dioxide, in contrast to speculations that tropical ecosystems were severely compromised by heat stress.

The Late Paleocene-Eocene Thermal Maximum [PETM, 56.3 million years ago (Ma)], lasting only ~100,000 to 200,000 years, was one of the most abrupt global warming events of the past 65 million years (*1*–*3*). The PETM is associated with a large negative carbon isotope excursion recorded in carbonate and organic materials, reflecting a massive release of ^{13}C-depleted carbon (*4*, *5*), an ~5°C increase in mean global temperature in ~10,000 to 20,000 years (*1*), a rapid and transient northward migration of plants in North America (*6*), and a mammalian turnover in North America and Europe (*7*).

Efforts to understand the impact of climate change on terrestrial environments have focused on mid- to high-latitude localities, but little is known of tropical ecosystems during the PETM. Tropical temperature change is poorly constrained, but, given the magnitude of temperature change elsewhere, tropical ecosystems are thought to have suffered extensively because mean temperatures are surmised to have exceeded the ecosystems' heat tolerance (*8*).

For this study, three tropical terrestrial PETM sites from Colombia and Venezuela were analyzed for pollen and spore content and stable carbon isotopic composition of organic materials (Fig. 1) (*9*). The analysis included 317 pollen samples, 1104 morphospecies, and 37,952 individual occurrences together with 489 carbon isotopes samples, 21 plant biomarker samples, and one radiometric age (*9*). Localities Mar 2X (core), Riecito Mache (outcrop), and Gonzales (outcrop and well) contain sediments that accumulated in fluvial to coastal plain settings. Biostratigraphy and carbon isotope stratigraphy, using bulk δ^{13}C and plant wax *n*-alkanes, confirm the position of the PETM at the three sites (Figs. 2 and 3) (*9*), which is not associated with any formation boundary or major lithological or depositional environment change. The location of the